AGU PUBLICATIONS

Journal of Advances in Modeling Earth Systems

RESEARCH ARTICLE

10.1002/2014MS000346

The Specified Chemistry Whole Atmosphere Community Climate Model (SC-WACCM)

K. L. Smith[1], R. R. Neely[2,3], D. R. Marsh[3], and L. M. Polvani[1,4]

[1]Division of Ocean and Climate Physics, Lamont-Doherty Earth Observatory, Palisades, New York, USA, [2]Advanced Study Program, National Center for Atmospheric Research, Boulder, Colorado, USA, [3]Atmospheric Chemistry Division, National Center for Atmospheric Research, Boulder, Colorado, USA, [4]Department of Applied Physics and Applied Mathematics and Department of Earth and Environmental Science, Columbia University, New York, New York, USA

Key Points:
- SC-WACCM is the new specified chemistry version of WACCM
- The climate and climate variability of SC-WACCM is nearly identical to WACCM
- The computational cost of SC-WACCM is roughly half that of WACCM

Correspondence to:
K. L. Smith,
ksmith@ldeo.columbia.edu

Citation:
Smith, K. L., R. R. Neely, D. R. Marsh, and L. M. Polvani (2014), The Specified Chemistry Whole Atmosphere Community Climate Model (SC-WACCM), *J. Adv. Model. Earth Syst.*, *6*, 883–901, doi:10.1002/2014MS000346.

Received 15 MAY 2014
Accepted 4 AUG 2014
Accepted article online 11 AUG 2014
Published online 28 AUG 2014

Abstract We here present, document and validate a new atmospheric component of the Community Earth System Model (CESM1): the Specified Chemistry Whole Atmosphere Community Climate Model (SC-WACCM). As the name implies, SC-WACCM is a middle atmosphere-resolving model with prescribed, rather than interactive chemistry. Ozone concentrations are specified throughout the atmosphere, using zonal and monthly mean climatologies computed by a companion integration with the Whole Atmosphere Community Climate Model (WACCM). Above 65 km, in addition, the climatological chemical and shortwave heating, nitrogen oxide, atomic and molecular oxygen and carbon dioxide are also prescribed from the companion WACCM integration. We carefully compare the climatology and the climate variability of preindustrial integrations of SC-WACCM and WACCM each coupled with active land, ocean and sea-ice components. We note some differences in upper stratospheric and lower mesospheric temperature, just below the 65 km transition level, due to the diurnal ozone cycle that is not captured when monthly mean ozone is used. Nonetheless, we find that the climatology and variability of the stratosphere, the troposphere and surface climate are nearly identical in SC-WACCM and WACCM. Notably, the frequency and amplitude of Northern Hemisphere stratospheric sudden warmings in the two integrations are not significantly different. Also, we compare WACCM and SC-WACCM to CCSM4, the "low-top" version of CESM1, and we find very significant differences in the stratospheric climatology and variability. The removal of the chemistry reduces the computational cost of SC-WACCM to approximately one half of WACCM: in fact, SC-WACCM is only 2.5 times more expensive than CCSM4 at the same horizontal resolution. This considerable reduction in computational cost makes the new SC-WACCM component of CESM1 ideally suited for studies of stratosphere-troposphere dynamical coupling and, more generally, the role of the stratosphere in the climate system.

1. Introduction

Over the past several decades, the global crisis of ozone depletion necessitated the development of general circulation models (GCMs) with a well-resolved stratosphere and interactive stratospheric ozone chemistry [*SPARC CCMVal*, 2010]. This focus has led to important advances in our understanding not only of ozone depletion and its projected recovery, but also of the unanticipated effects of ozone depletion on climate, particularly in the Southern Hemisphere [see *Thompson et al.*, 2011; *Previdi and Polvani*, 2014, for recent reviews].

Unfortunately, model integrations of stratosphere-resolving GCMs with interactive chemistry are computationally expensive. For example, the National Center for Atmospheric Research (NCAR) Whole Atmosphere Community Climate Model (WACCM) of the Community Earth System Model Version 1 (CESM1) includes 59 chemical species, 217 gas-phase reactions and 17 heterogenous reactions, and requires 1130 core-hours per year of integration on the NCAR Yellowstone supercomputer using 352 processors (Table 3).

For scientists interested in studying the dynamics—rather than the chemistry—of the stratosphere and its coupling to surface climate, the substantial resources required to run interactive chemistry has limited the extent to which models, such as WACCM, are used for dynamical studies. Although stratospheric dynamics and ozone chemistry and transport [*Tegtmeier et al.*, 2008] are inherently coupled, it is currently unclear whether this coupling is strong enough to initiate feedbacks that significantly alter the climate and/or

variability of the stratospheric circulation, or tropospheric climate, or whether prescribing ozone as a radiative forcing is sufficient to represent ozone effects on climate and its variability. One way to answer this is to compare model integrations with and without interactive chemistry.

The comparison of model integrations with and without interactive middle atmosphere chemistry reflects three important differences in the treatment of ozone: (1) fully time-varying versus monthly mean climatological ozone, (2) zonally asymmetric versus zonal mean ozone, and (3) dynamically consistent feedbacks between the atmospheric circulation and ozone chemistry. While the relative importance of these three factors is unclear, several studies have shown that a more realistic representation of lower stratospheric ozone in model integrations, particularly zonal asymmetries in stratospheric ozone, has a significant impact on the stratospheric circulation [*Gabriel et al*., 2007; *Crook et al*., 2008; *Gillett et al*., 2009; *Waugh et al*., 2009; *McCormack et al*., 2011; *Albers and Nathan*, 2012; *Albers et al*., 2013] and some also show that this couples downward and subsequently affects the tropospheric circulation [*Crook et al*., 2008; *Waugh et al*., 2009].

Aiming at a better understanding of chemistry-climate coupling, in this study we introduce SC-WACCM, a new specified chemistry (SC) configuration of WACCM. Rather than solving for the concentration of ozone and other chemical species interactively, as in WACCM, ozone together with chemical and shortwave heating rates are simply prescribed in SC-WACCM. In this paper, we focus on describing and validating SC-WACCM, and so limit our analysis to preindustrial integrations. In a future paper, we will examine the effect of prescribed versus interactive chemistry on the Southern Hemisphere climate during the historical period of ozone depletion.

This paper is laid out as follows. In section 2, we describe the new model and, in section 3, we outline the model integrations that will be analyzed. Section 4 presents the model validation in four subsections: ozone and heating rates in section 4.1, the zonal mean climate in section 4.2, the surface climate in section 4.3 and the climate variability in section 4.4. We discuss the computational costs of SC-WACCM in section 5 and, finally, in section 6, we summarize our findings and conclude.

2. Model Description

SC-WACCM is part of the NCAR Community Earth System Model (CESM) [*Hurrell et al*., 2013]. The atmospheric component of the model is a modified version of CESM1(WACCM) [*Marsh et al*., 2013], the stratosphere-resolving (i.e., "high-top"), coupled-middle atmosphere chemistry version of CESM1, hereafter referred to as WACCM. SC-WACCM has the same 66 vertical levels and horizontal resolution (1.9° latitude by 2.5° longitude) as WACCM, and the model lid remains at 5.1×10^{-6} hPa (approximately 140 km). In the integrations presented here, SC-WACCM is coupled to identical interactive land, ocean, and sea ice models as in the WACCM integrations conducted as part of the Coupled Model Intercomparison Project Phase 5 (CMIP5) described in *Marsh et al*. [2013]. Both models include the same parameterization of nonorographic gravity waves (generated by frontal systems and convection), and also the parameterized surface stress due to unresolved topography, referred to as turbulent mountain stress, or TMS [*Richter et al*., 2010]. The parameterized auroral oval, an important source of nitrogen oxide (NO) above 100 km, is omitted in SC-WACCM for computational efficiency, but NO is prescribed from WACCM integrations that do include this source (see below).

In describing the configuration of SC-WACCM, we start by distinguishing two regions, in which the effects of middle atmosphere radiation and chemistry are treated differently. These regions are merged together via a hyperbolic tangent weighting function from approximately 63–70 km altitude [*Neale et al*., 2012]. Figure 1a shows the vertical resolution of WACCM/SC-WACCM and highlights these two regions. The overlap region is shaded in gray. We also note that all prescribed fields are specified globally at a frequency determined by the input data file, and in this study we use monthly mean, zonal mean values from a prior integration of WACCM.

In the lower region, shortwave heating and longwave cooling rates are computed by passing the concentrations of radiatively active atmospheric constituents (water vapor (H_2O), carbon dioxide (CO_2), methane (CH_4), ozone (O_3), nitrous oxide (N_2O), CFC-11 and CFC-12) to the same radiative transfer code (CAM-RT) [*Collins et al*., 2004] used in the "low-top" Community Climate System Model Version 4 (CCSM4) [*Gent et al*., 2011]. Note that ozone concentrations are prescribed in *both* regions in SC-WACCM from a prior integration of WACCM and, in the lower region, the concentration of CO_2 is specified by a single, uniform value.

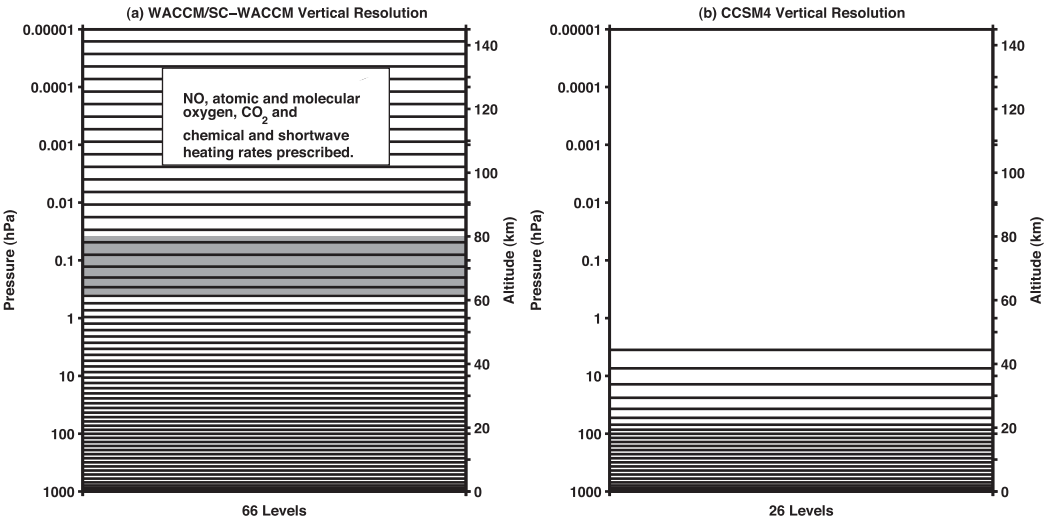

Figure 1. Hybrid model levels for (a) WACCM/SC-WACCM and (b) CCSM4. In SC-WACCM, in the lower region, shortwave and longwave heating rates are calculated as in CCSM4, while in the upper region longwave heating rates are calculated as in WACCM and chemical and shortwave heating rates (QRS) are prescribed from a prior integration of WACCM. The overlap region from 63 to 70 km, over which heating and cooling rates are merged between WACCM/SC-WACCM and CCSM4, is shaded gray in Figure 1a. In SC-WACCM, monthly mean, zonal mean ozone from a companion WACCM integration is prescribed everywhere and, like QRS, monthly mean, zonal mean NO, atmoic and molecular oxygen (O and O_2), CO_2 are prescribed only above the overlap region.

In the upper region, in addition to ozone, NO, atomic and molecular oxygen (O and O_2), CO_2—which are required to calculate the longwave cooling rates—and chemical and shortwave heating rates are prescribed from the prior integration of WACCM. As mentioned above, in the lower region, it is sufficient to prescribe the concentrations of radiatively active gases for the radiative transfer calculation of the instantaneous shortwave heating rates from the divergence of the solar radiative flux. However, this is not the case in the upper region, which corresponds to the mesosphere and lower thermosphere (MLT), where the majority of heating comes from exothermic chemical reactions rather than absorption of shortwave radiation [*Mlynczak and Solomon*, 1993]. The solar energy necessary to break molecular bonds during photolysis is returned as heat during recombination reactions, but this reaction may occur at a different location and possibly long after the initial molecule was photolysed.

For example, atomic oxygen produced by the photolysis of molecular oxygen has a chemical lifetime of months near the mesopause [*Brasseur and Solomon*, 2005]. Further complicating matters is that the constituents participating in these reactions can have large diurnal cycles such that large errors would be introduced if zonal and/or monthly mean quantities were used to calculate heating rates. Since it would be prohibitive to prescribe the continuously changing diurnal concentrations of *all* chemical species that participate in exothermic reactions, in SC-WACCM we simply prescribe the zonal and monthly mean of the sum of these chemical heating rates in the MLT rather than the constituent concentrations themselves.

In addition, constituents involved in the absorption of shortwave radiation, such as ozone, also have large diurnal cycles in the MLT and, thus, the shortwave heating rates due to the gaseous absorption by ozone, CO_2, and water vapor are also prescribed. Finally, the zonal mean heating from the directly thermalized energy realized during photolysis, photoabsorption and photoionization, and during energetic particle precipitation in the aurora [*Marsh et al*., 2007] is also specified in the MLT in SC-WACCM, rather than explicitly simulating these processes interactively as in WACCM. This ensures that the total energy input into SC-WACCM at each pressure level is, on average, nearly identical to the fully interactive version (WACCM). As will be shown below, this procedure results in good agreement between WACCM and SC-WACCM in the mean thermal structure of the atmosphere.

Unlike the chemical and shortwave heating rates, longwave cooling rates in the upper region are not prescribed, since they depend on temperature as well as constituent concentrations. In SC-WACCM, therefore, the concentrations of O_3, NO, O, O_2 and CO_2 in this region are read in from the prior WACCM integration and passed, along with temperature, to the same radiative transfer routines used in WACCM for the

calculation of nonlocal thermodynamic equilibrium (LTE) cooling rates. Cooling by NO at 5.3 μm and CO_2 in the 15 μm band are calculated using the formulations by *Kockarts* [1980] and *Fomichev et al*. [1998], respectively.

In addition to O_3, NO, O, O_2 and CO_2, the computation of longwave radiative transfer in the upper region requires the concentrations of H_2O, CH_4, N_2O, CFC-11 and CFC-12 [*Collins et al*., 2004]. In SC-WACCM, these are all prognostic constituents. The concentrations of these prognostic species (except H_2O) are specified at the surface, as in WACCM, and are taken from *Meinshausen et al*. [2011]. They are then transported by the calculated wind field, and are removed from the model at a rate that varies with month, latitude and model pressure level. These loss rates are taken from the Garcia and Solomon two-dimensional model, [*Garcia and Solomon*, 1994] and their annual and global mean values are shown in Figure 2.

In order to retain the effects of methane oxidation in the middle atmosphere in the absence of prognostic chemistry, we use the following approximation: for each CH_4 lost, two H_2O molecules are produced. The middle atmosphere water vapor concentration in SC-WACCM is, therefore, a balance between production by CH_4 oxidation and loss by photolysis. The loss rate of water vapor by photolysis is shown in Figure 2.

To summarize: as in WACCM, the shortwave heating rates and longwave cooling rates above and below the overlap region, are combined smoothly via a hyperbolic tangent weighting function, such that SC-WACCM is energetically consistent with WACCM. All other design aspects of SC-WACCM are the same as WACCM. Additional technical details about the WACCM design can be found in an NCAR Technical Note entitled, Description of the Community Atmosphere Model CAM 5.0 [*Neale et al*., 2012].

3. Description of Model Integrations

As part of CMIP5, NCAR produced a 200 year long 1850 preindustrial integration for WACCM [*Marsh et al*., 2013]. The well-mixed greenhouse gases, ozone-depleting substances and aerosol forcings in this preindustrial integration were all set to their 1850 values, the solar constant was set to solar average, and no volcanic eruptions or prescribed QBO were included. To evaluate SC-WACCM, we completed a new 200 year long preindustrial integration of the model. Monthly and daily time resolution output was saved for both of these integrations.

In this study, we will also briefly compare the WACCM and SC-WACCM preindustrial integrations to the CMIP5 CCSM4 preindustrial integration. CCSM4 has 26 vertical levels and a model top at 2.2 hPa (see Figure 1b). The standard horizontal resolution of CCSM4 is $0.9^\circ \times 1.25^\circ$ which is finer than WACCM. In addition to the inclusion of a nonorographic gravity wave parameterization in WACCM/SC-WACCM, one other key difference between the WACCM/SC-WACCM and CCSM4 configurations is the specification of the turbulent mountain stress (TMS); the TMS parameterization is switched on in WACCM/SC-WACCM but is off in CCSM4.

Other than the items discussed above, WACCM, SC-WACCM, and CCSM4 all use the same representation of physical processes in the troposphere, and are coupled to identical land, ocean and sea ice components. Only the atmospheric components differ in these models. Five hundred years of monthly preindustrial data, along with 54 years of daily data are available for CCSM4. CCSM4 uses prescribed preindustrial ozone forcing from a preindustrial integration of CAM-CHEM, which includes a simplified representation of stratospheric ozone chemistry [*Lamarque et al*., 2012].

Note that some, but not all, of the differences between the WACCM/SC-WACCM and CCSM4 integrations presented below result from differences in vertical resolution and model top. In particular, differences in TMS and horizontal resolution also likely contribute to model differences, chiefly at the surface. In providing diagnostics for CCSM4, our intention is not to attribute each of the differences between WACCM/SC-WACCM and CCSM4 to specific differences in model configuration. Rather, the CCSM4 comparisons are simply meant to demonstrate the differences between the "high-top" versions of the CESM1 family (WACCM and SC-WACCM), and the more widely used "low-top" version, CCSM4.

Many of the plots in the sections below show the difference between WACCM and SC-WACCM, i.e., for some field X, we show $\Delta X = X_{WACCM} - X_{SC-WACCM}$. We assess the statistical significance of ΔX using a Student's *t* test, and of differences in probability density distributions using a Kolmogorov-Smirnov (K-S) test.

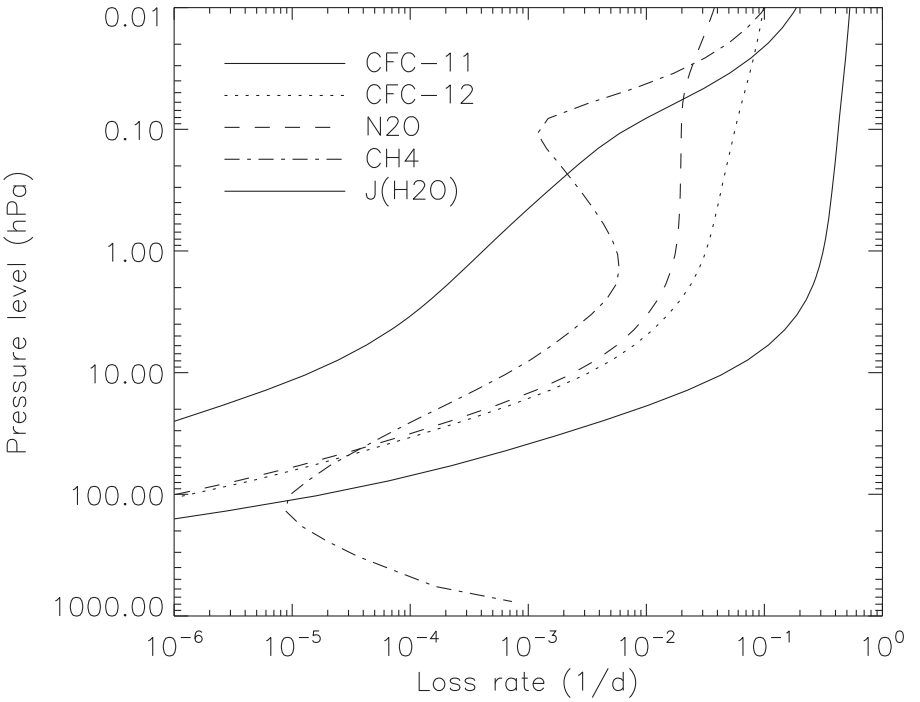

Figure 2. Annual and global mean of loss rates specified for prognostic constituents in SC-WACCM.

4. Model Comparison

4.1. Ozone and Heating Rates

Figure 3 shows the total column-integrated ozone as a function of month and latitude averaged over the 200 year preindustrial WACCM integration. Most of the ozone in the column is located below the overlap region and is therefore more representative of the input to the CAM4 radiative transfer module, CAM-RT. Figure 3 shows the peak in ozone in the winter/spring in both the Northern and Southern Hemisphere extratropics associated with ozone transport by the Brewer-Dobson circulation. The Northern Hemisphere extratropics has a substantially larger peak due to greater wave-induced transport by the Brewer-Dobson circulation while the stable and cold Southern Hemisphere polar vortex is much more isolated. Figure 3 also demonstrates the tropical minimum in ozone due to photolytic destruction of ozone in this region.

Relative to present-day ozone from the CMIP5 WACCM historical integrations, preindustrial ozone concentrations are approximately 50–60% greater in the Antarctic spring and 10–15% greater in the Arctic spring due to ozone depletion caused by anthropogenic chlorofluorocarbon emissions. In the tropics, ozone concentrations are approximately 5% lower in preindustrial times due to increased emission of tropospheric ozone precursors in present-day.

Although there is limited documentation of preindustrial ozone simulated by other coupled-chemistry models, *Lamarque et al*. [2011] and *Young et al*. [2013] offer some analysis of preindustrial and present-day ozone, primarily tropospheric, in the Atmospheric Chemistry and Climate Model Intercomparison Project (ACCMIP) model integrations. Both studies show an increase in tropospheric ozone and a decrease in stratospheric ozone from preindustrial to present-day. This is consistent with what we see in WACCM.

As described earlier, in the upper region, the total chemical and shortwave heating rate, QRS, is prescribed in SC-WACCM using a climatology created from the full preindustrial WACCM integration. Figure 4a shows the annual mean, zonal mean QRS from WACCM. QRS peaks in the upper atmosphere where absorption of solar radiation by molecular oxygen is the main source of energy. There is a secondary maximum near the stratopause (near 1 hPa) due to absorption by ozone. Although the ozone concentration peaks in the lower stratosphere, absorption of shortwave radiation starting at the top of the ozone layer leads to less radiation available for absorption at lower altitudes.

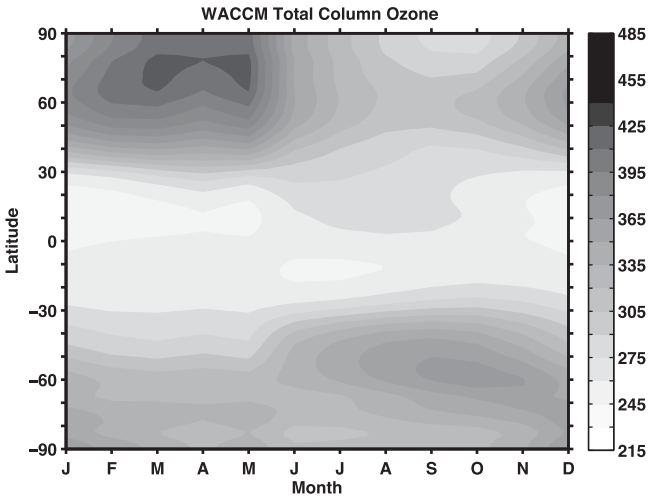

Figure 3. Climatological monthly and zonal mean WACCM preindustrial total column ozone in Dobson Units (DU).

Figure 4b shows the difference in annual mean, zonal mean QRS between WACCM and SC-WACCM. In the upper region, QRS is identical in the two integrations, as would be expected (recall Figure 1a). In addition, in much of the troposphere and lower stratosphere, there is no significant difference between the annual mean QRS of the two models. However, immediately below the overlap region, significant differences arise as an artifact of the diurnal averaging that occurs when using monthly mean ozone input data in SC-WACCM. In WACCM, the full diurnal cycle of ozone is computed. The diurnal cycle amplitude increases with height, with maximum ozone concentrations at night and minimum concentrations during the day. Since monthly mean ozone is prescribed in SC-WACCM, there is no ozone diurnal cycle. Consequently, ozone concentrations are larger during daylight hours in SC-WACCM than in WACCM, increasing shortwave absorption, and causing the negative difference in QRS in the lower mesosphere in Figure 4b. This issue was first pointed out by *Sassi* [2005] in an earlier study of WACCM with prescribed ozone. The region of positive ΔQRS directly below the region of negative ΔQRS results from greater absorption in the lower mesosphere and upper stratosphere in SC-WACCM allowing the availability of less short-wave radiation for absorption below.

Figure 4c shows ΔQRS but now in terms of percentage difference. Throughout most of the lower stratosphere and troposphere, the percentage differences are less than $\pm 5\%$. In the lower mesosphere, this plot highlights the magnitude of the effect of the ozone diurnal cycle on the shortwave heating rate. The percentage difference is as large as -55% in the lower meosphere.

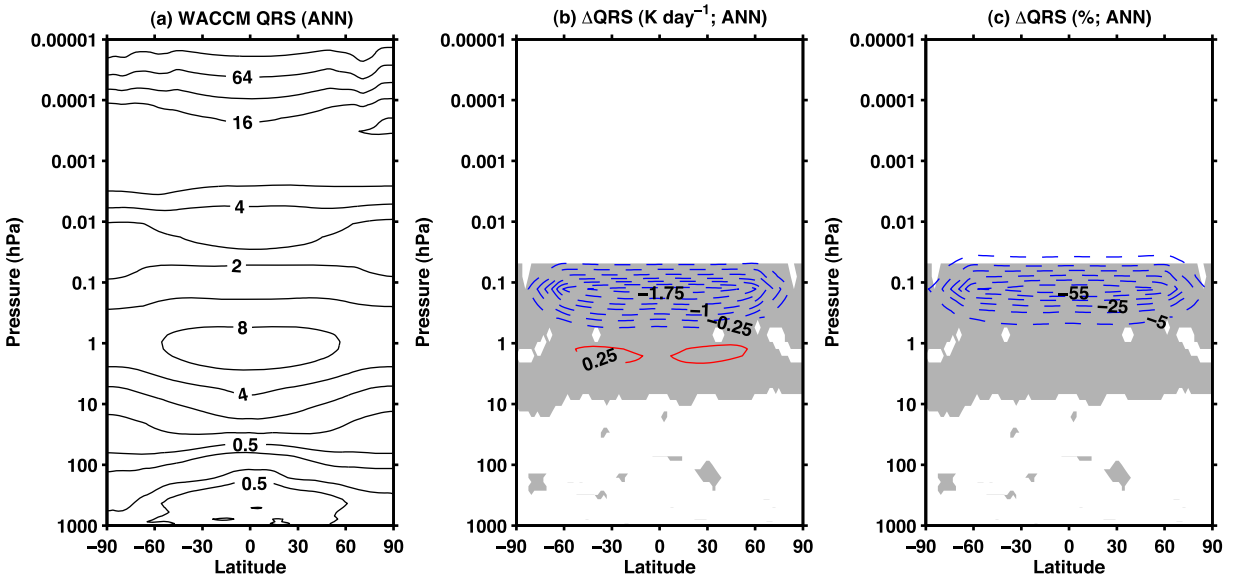

Figure 4. Annual and zonal mean (a) total chemical and shortwave heating rate (QRS) for WACCM in K d^{-1}, (b) Δ QRS_TOT (WACCM minus SC-WACCM) in K d^{-1} and (c) Δ QRS in %. Red (blue) contours are positive (negative) values. Contour interval is 2^{-2}, 2^{-1}, 1, 2, 2^2,… K d^{-1} in Figure 4a, 0.25 K d^{-1} in Figure 4b, and…, −25, −15, −5, 5, 15, 25,… in Figure 4c. Gray shading indicates regions that are significantly different at the 95% level.

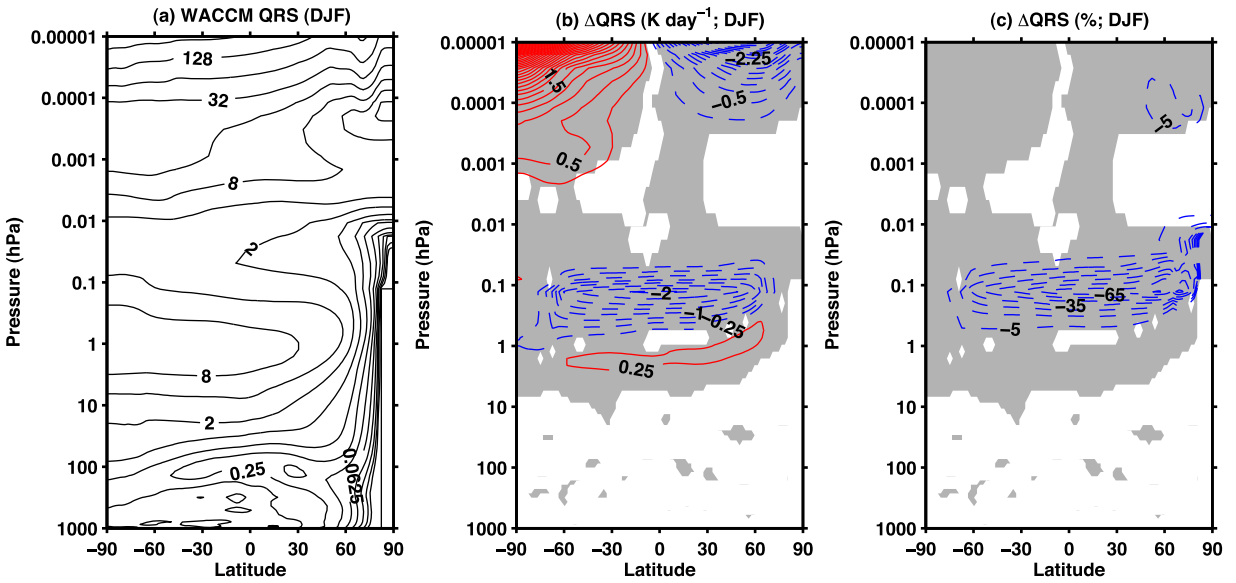

Figure 5. As in Figure 4 but for December-January-February (DJF).

Figure 5 shows the same fields as Figure 4 except for the December-January-February (DJF) season. Figure 5a illustrates the need to prescribe QRS in SC-WACCM rather than simply prescribing ozone alone. In the winter hemisphere there is no shortwave heating in the polar troposphere, stratosphere and lower mesosphere due to lack of insolation; however, in the upper atmosphere, chemical heating is nonzero and contributes to QRS.

The annual mean shown in Figure 4 masks another issue with prescribing monthly mean fields in SC-WACCM. Figure 5b shows ΔQRS for DJF. The linear interpolation of WACCM QRS from monthly resolution to the model time step within SC-WACCM essentially causes a weakening of the amplitude of the seasonal cycle of QRS in SC-WACCM relative to WACCM. While in the annual mean this smoothing averages out, the effect is quite evident in the winter and summer seasons in the thermosphere. However, because the climatological heating rates are so large in this region, the magnitude of the percentage difference in QRS in the upper atmosphere amounts to less than $\pm 5\%$ (Figure 5c).

4.2. Zonal Mean Climate

In this section, we examine the differences in the zonal mean climate. Because we are focusing on preindustrial integrations, we do not include comparisons between model integrations and satellite and reanalysis data. The reader is referred to *Marsh et al.* [2013] for comparisons between WACCM and observational data for the historical period. We assume that any differences between WACCM and SC-WACCM in the preindustrial epoch carry over to the present-day.

First we examine the differences in zonal mean temperature between WACCM and SC-WACCM. For the remainder of the paper, we will limit our analysis to the troposphere, stratosphere and lower mesosphere, i.e., from the surface to 0.01 hPa (approximately 80 km). Figures 6a and 6b show the differences in temperature for DJF and June-July-August (JJA). Not surprisingly, the largest differences in temperature are associated with the largest differences in QRS (Figure 5b). Temperature is approximately 8–9° warmer in SC-WACCM than in WACCM in the tropical lower mesosphere. Despite this, temperatures throughout much of the troposphere and lower stratosphere are not significantly different and are less than 1 K, corresponding to percentages differences of less than $\pm 2\%$.

Figure 6c and 6d show the differences in zonal mean zonal winds. The zonal wind differences in the lower mesosphere are roughly in thermal wind balance with the temperature differences. However, throughout much of the lower stratosphere and troposphere, the zonal winds are not significantly different. In spite of the large temperature differences and smaller zonal wind differences near 0.1 hPa, it is important to recall that most planetary waves are dissipated below this level. Thus, the differences at 0.1 hPa between WACCM

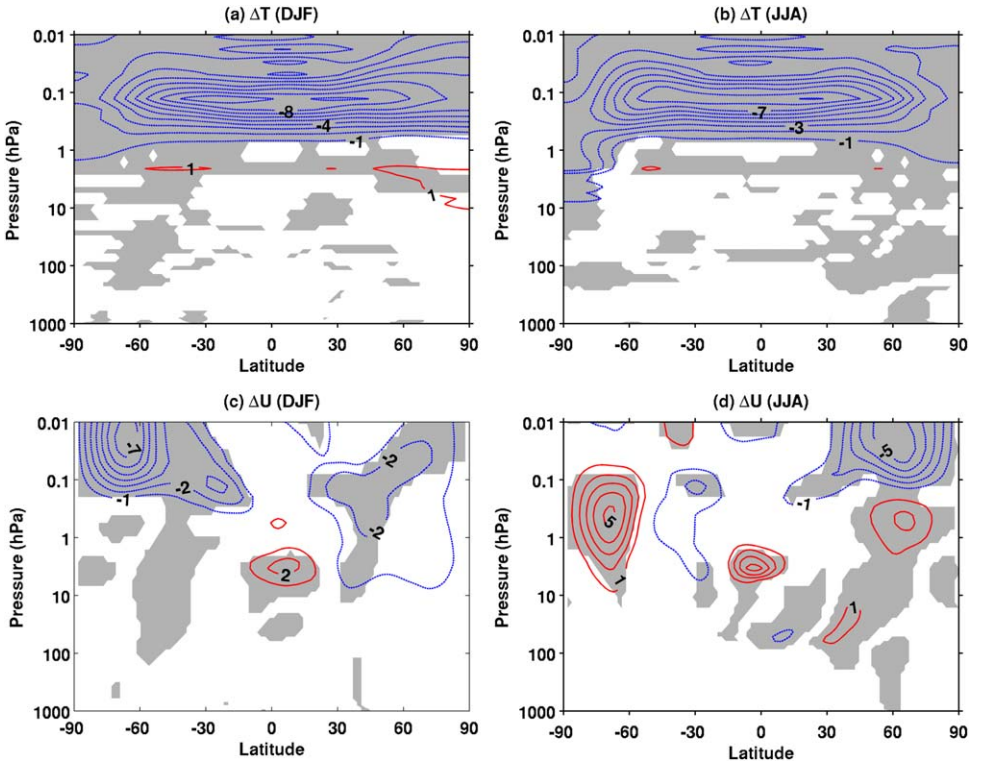

Figure 6. Difference (WACCM minus SC-WACCM) in (a, b) zonal mean temperature and (c, d) zonal wind for December-January-February (DJF) (Figures 6a and 6c) and June-July-August (JJA) (Figures 6b and 6d). Red (blue) contours are positive (negative) values. Contour intervals are 1 K and 1 m s^{-1}. Gray shading indicates regions that are significantly different at the 95% level.

and SC-WACCM likely have little effect on planetary wave propagation and, thus, little downward influence on the climate below.

For completeness, we also show the full zonal mean temperature (Figure 7) and zonal wind (Figure 8) fields for WACCM, SC-WACCM and CCSM4 for DJF and JJA. The black horizontal line in the WACCM/SC-WACCM panels in Figures 7 and 8 correspond to the highest model pressure level in CCSM4 (see also Figure 1). Like Figures 6a and 6b, Figures 7a and 7b show that SC-WACCM is slightly warmer than WACCM in the lower mesosphere. The largest difference between CCSM4 and the other two models is that both the winter and summer polar stratospheric temperatures are colder in CCSM4.

Figure 8 shows that despite the differences shown in Figure 6, the Arctic polar vortex looks remarkably similar in WACCM and SC-WACCM in DJF; however, the vortex is much stronger in CCSM4 (compare CCMS4 to WACCM/SC-WACCM just below the black horizontal lines). This is a common bias in "low-top" models that do not realistically represent stratospheric variability, such as stratospheric sudden warmings (SSWs) [*Charlton-Perez et al*., 2013]. SSWs will be discussed further in Section 4.4. In JJA, the Antarctic polar vortex again looks very similar in WACCM and SC-WACCM and is somewhat weaker than CCSM4. This is likely due to the differences in the gravity wave drag treatment near the model lid, i.e., CCSM4 employs Rayleigh drag in the sponge layer.

We are particularly interested in how well SC-WACCM simulates the stratospheric circulation in order to validate the model's utility for studies of stratospheric dynamics and stratosphere-troposphere coupling. To examine the seasonal cycle of the polar vortices, Figure 9 shows the zonal mean zonal winds at 60°N and 60°S and at 10 hPa for WACCM (black curve), SC-WACCM (red curve) and CCSM4 (blue curve). Figure 9a shows that the zonal mean zonal winds are not significantly different between WACCM and SC-WACCM throughout the entire year. As also shown in Figure 8e, the CCSM4 winds are significantly stronger throughout most of the year, indicative of a cold and stable vortex and the lack of stratospheric variability, such as SSWs.

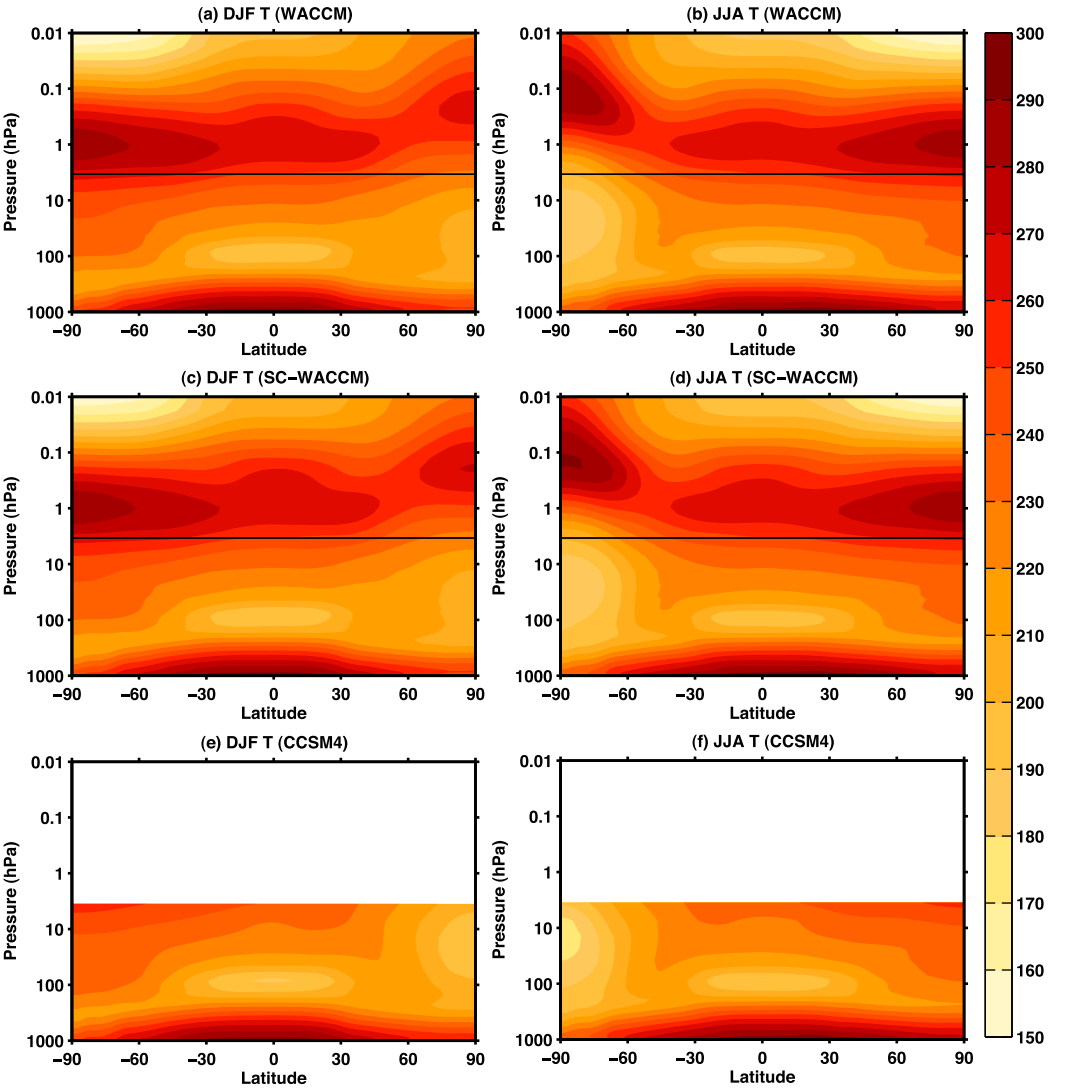

Figure 7. Zonal mean temperature for (a, c, e) December-January-February (DJF) and (b, d, f) June-July-August (JJA). Figures 7a and 7b are for WACCM, Figures 7c and 7d are for SC-WACCM and Figures 7e and 7f are for CCSM4. Shading interval is 10 K.

Figure 9b shows the standard deviation of the zonal mean zonal winds at 60°N and at 10 hPa for WACCM (black curve), SC-WACCM (red curve) and CCSM4 (blue curve). The standard deviation for WACCM and SC-WACCM is very similar throughout the seasonal cycle. CCSM4 shows weaker variability in the winter months, consistent with weaker wave driving (see Section 4.4 below).

In the Southern Hemisphere, there is very little difference in the seasonal evolution of the polar vortex between WACCM and SC-WACCM (Figure 9c), whereas the Antarctic polar vortex in CCSM4 is significantly weaker throughout the year. This may reflect the presence of Rayleigh drag in the sponge layer in CCSM4. As above, Figure 9d shows the standard deviation for WACCM (black curve), SC-WACCM (red curve) and CCSM4 (blue curve). The black and red curves are again very similar while the blue curve shows larger variability in CCSM4, particularly in spring, likely due to the weaker vortex which is, consequently, more easily perturbed.

Another important diagnostic of stratospheric dynamics and transport is the Brewer-Dobson circulation (BDC). Figure 10 shows the Transformed Eulerian Mean (TEM) vertical velocity, w*, in DJF, for WACCM, SC-WACCM and CCSM4 at 100, 50 and 20 hPa. As expected, WACCM and SC-WACCM are indistinguishable. Downward control calculations show that the contributions to tropical upwelling by resolved and

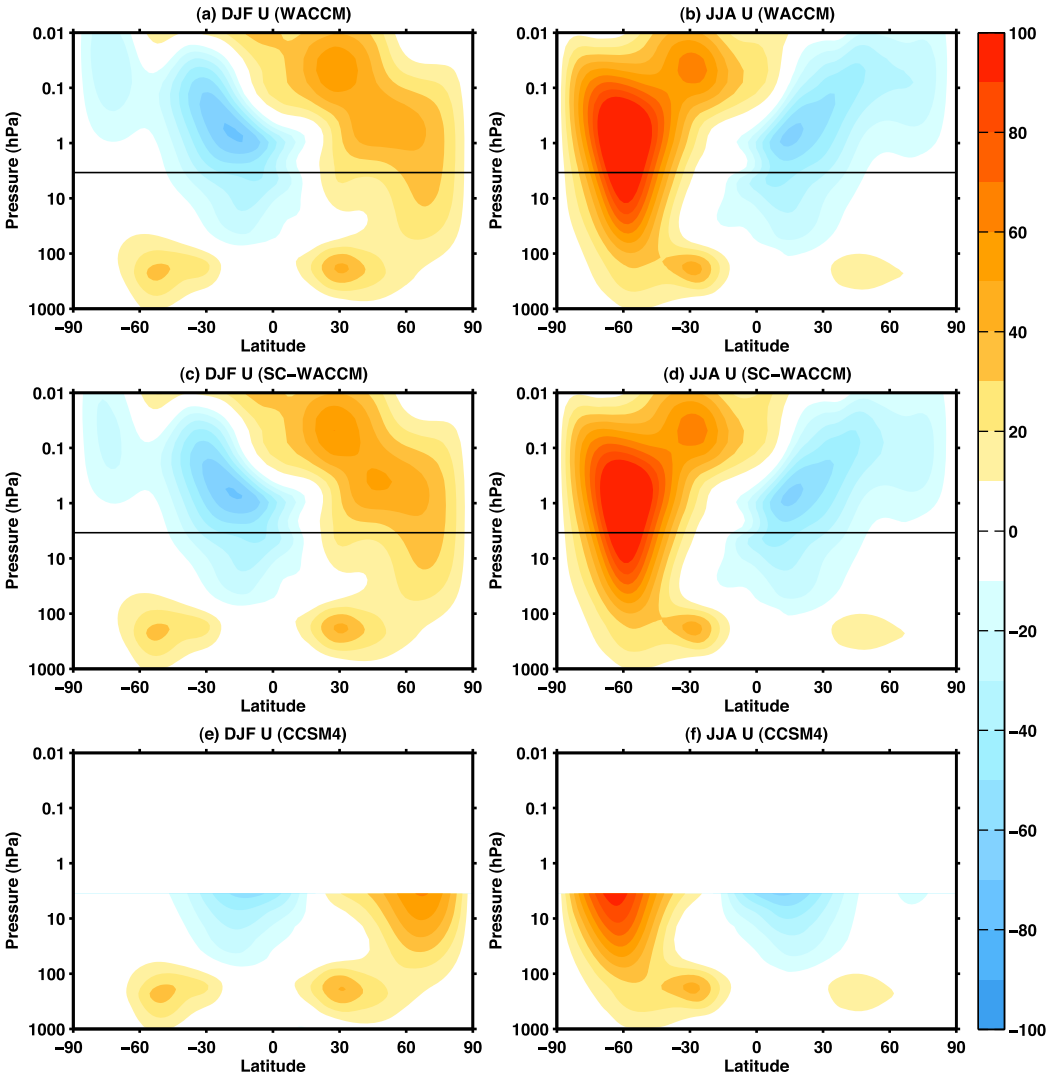

Figure 8. Zonal mean zonal wind for (a, c, e) December-January-February (DJF) and (b, d, f) June-July-August (JJA). Figures 8a and 8b are for WACCM, Figures 8c and 8d are for SC-WACCM and Figures 8e and 8f are for CCSM4. Shading interval is 10 m s^{-1}.

parameterized waves is also very similar [not shown; *Haynes et al*., 1991; *Garcia and Randel*, 2008]. In contrast, CCSM4 shows much weaker downwelling in the Northern Hemisphere extratropics as a consequence of relatively weaker wave-driving. For more information on the BDC in twentieth century WACCM integrations see *Butchart et al*. [2010] and *Hardiman et al*. [2013].

Finally, we examine how well SC-WACCM simulates the tropical water vapor tape recorder in the upper troposphere-lower stratosphere (UTLS) region. Figures 11a–11c show the anomaly in water vapor, averaged from 10°S to 10°N as a function of month and pressure for WACCM, SC-WACCM, and CCSM4, respectively. WACCM and SC-WACCM simulate a very similar seasonal cycle of UTLS tropical water vapor, while CCSM4 is significantly different. Although this comparison applies to preindustrial integrations, Figure 11 confirms that WACCM and SC-WACCM do a reasonable job of simulating the seasonal variation in UTLS tropical water vapor relative to observations (as shown in *SPARC CCMVal* [2010]). The large differences between WACCM/SC-WACCM and CCSM4 are mainly due to differences in cloud parameterizations, (e.g., the cloud relative humidity threshold and ice particle fall velocities) rather than differences in tropical upwelling (Figure 10). These cloud parameters were specifically tuned in WACCM to improve the simulation stratospheric water vapor. However, greater vertical resolution in the UTLS region may also contribute to the superior simulation of the tropical tape recorder in WACCM/SC-WACCM relative to CCSM4.

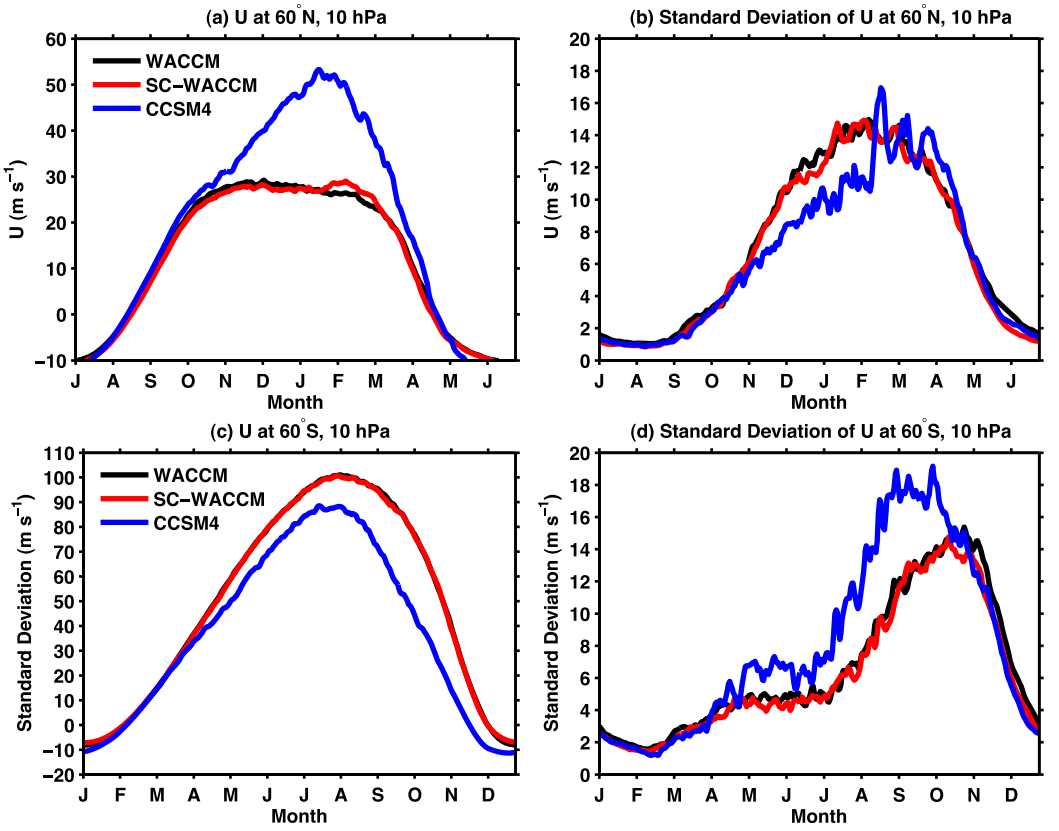

Figure 9. Daily zonal mean zonal wind at 10 hPa and (a) 60°N and (c) 60°S for WACCM (black), SC-WACCM (red), and CCSM4 (blue) as a function of month. (b, d) as Figures 9a and 9b but for the standard deviation of the zonal mean zonal wind.

In summary, we find that issues arising from the diurnal cycle of ozone lead to some differences in zonal mean temperatures and winds in the lower mesosphere between WACCM and SC-WACCM. However, these differences appear to have a very small effect on the winds and temperatures in the lower stratosphere and free troposphere, the stratospheric polar vortices, the BDC and UTLS tropical water vapor. Relative to CCSM4, the climatology of the stratosphere and troposphere in WACCM and SC-WACCM are practically indistinguishable.

4.3. Surface Climate

In this section, we compare the surface climate in WACCM and SC-WACCM. Table 1 lists the mean ± two standard deviations for annual mean surface air temperature (*SAT*), precipitation (*PRECIP*), sea-level pressure

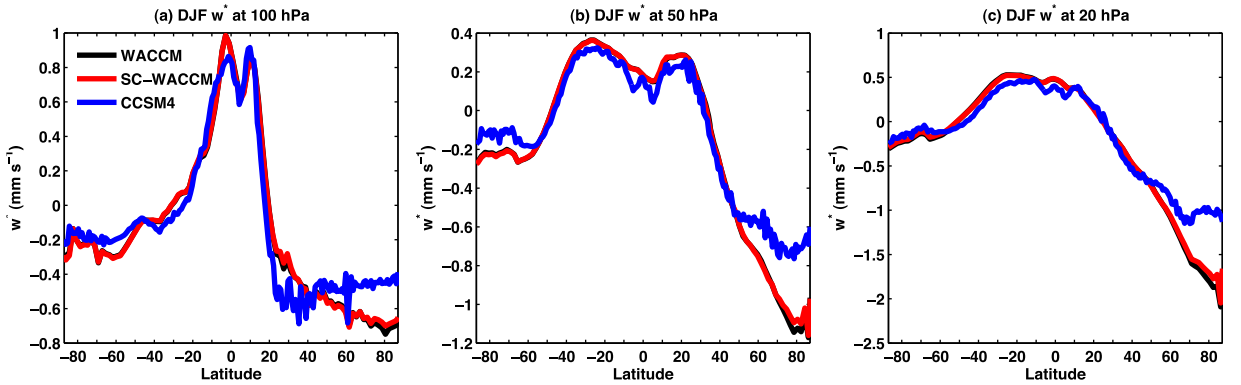

Figure 10. December-January-February (DJF) zonal mean w* in mm s^{-1} at (a) 100 hPa, (b) 50 hPa, and (c) 20 hPa for WACCM (black), SC-WACCM (red) and CCSM4 (blue).

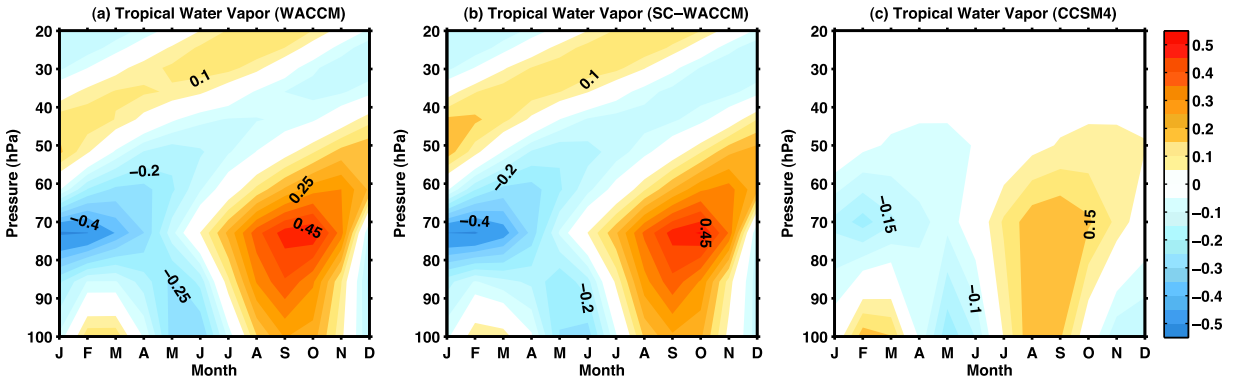

Figure 11. Water vapor tape recorder signal in (a) WACCM, (b) SC-WACCM, and (c) CCSM4. Plots show the water vapor anomaly (ppmv) from the time-mean averaged over 10°S – 10°N.

(*SLP*) and sea ice extent (*SIE*) for WACCM, SC-WACCM and CCSM4 for the global mean, the Northern Hemisphere extratropics (21°N–90°N), the tropics (21°S–21°N) and the Southern Hemisphere extratropics (21°S–90°S).

WACCM and SC-WACCM are not significantly different across all fields and all latitude bands. The differences between WACCM and CCSM4 are discussed in detail in *Marsh et al.* [2013], but here we highlight the largest differences. CCSM4 is slightly colder than WACCM and SC-WACCM in the Southern Hemisphere extratropics due to significantly more extensive Antarctic sea ice. CCSM4 also has significantly less extensive sea ice in the Arctic. Precipitation is larger in all latitude bands in CCSM4, and SLP is different in the tropics and Northern Hemisphere extratropics. The differences in precipitation and *SLP* likely reflect differences in horizontal resolution, and the inclusion of the TMS parameterization in WACCM and SC-WACCM. For twentieth century integrations, *Marsh et al.* [2013] examined the sensitivity of precipitation and *SLP* in CCSM4 to horizontal resolution and TMS by using the same settings used in WACCM (WSET). They found no significant difference in these surface fields between the WACCM and CCSM4-WSET integrations. Moreover, differences in sea ice extent have also been attributed to the TMS parameterization [*Marsh et al.*, 2013].

Figures 12a–12c show the *SAT* as a function of month for WACCM, SC-WACCM and CCSM4 for the global mean, the Northern Hemisphere polar cap (60°N–90°N), and the Southern Hemisphere polar cap (60°S–90°S). Months when WACCM and CCSM4 are not significantly different are highlighted with gray shading. As is Table 1, WACCM and SC-WACCM are not significantly different across all latitude bands. In the global mean, CCSM4 is significantly colder than WACCM and SC-WACCM. This is primarily due to a colder Southern Hemisphere extratropics in CCSM4 due to the greater extent of Antarctic sea ice. Figure 12c shows that over the Southern Hemisphere polar cap, the largest differences between WACCM and CCSM4 occur in the winter months, when sea ice is most extensive. The significantly warmer temperatures in CCSM4 relative to

Table 1. WACCM, SC-WACCM, and CCSM4 Annual Mean Surface Air Temperature (*SAT*), Precipitation (*PRECIP*), Sea-Level Pressure (*SLP*), and Sea Ice Extent (*SIE*) for Preindustrial Conditions[a]

	Model	*SAT* (*K*)	*PRECIP* (mmd^{-1})	*SLP* (hPa)	*SIE* (10^{6}km^2)
Global	WACCM	286.8 (0.2)	2.83 (0.03)	1011.3 (0.05)	
	SC-WACCM	286.8 (0.3)	2.82 (0.03)	1011.3 (0.05)	
	CCSM4	286.5 (0.2)	2.93 (0.02)	1011.2 (0.04)	
21°–90°N	WACCM	281.1 (0.3)	2.00 (0.04)	1016.9 (0.4)	14.0 (0.6)
	SC-WACCM	281.0 (0.3)	2.00 (0.05)	1017.0 (0.5)	14.0 (0.5)
	CCSM4	281.0 (0.3)	2.13 (0.04)	1014.9 (0.5)	13.3 (0.5)
21°S–21°N	WACCM	298.2 (0.4)	4.10 (0.08)	1010.6 (0.4)	
	SC-WACCM	298.2 (0.5)	4.09 (0.07)	1010.6 (0.4)	
	CCSM4	298.2 (0.4)	4.20 (0.07)	1011.9 (0.3)	
21°–90°S	WACCM	279.9 (0.2)	2.25 (0.04)	1006.6 (0.4)	16.4 (0.9)
	SC-WACCM	279.9 (0.2)	2.25 (0.04)	1006.5 (0.4)	16.5 (0.7)
	CCSM4	279.0 (0.2)	2.33 (0.04)	1006.7 (0.4)	20.4 (1.1)

[a]Climatological means are calculated over 200 years for WACCM, 200 years for SC-WACCM and 500 years for CCSM4. The 2σ uncertainties in the means are listed in parentheses.

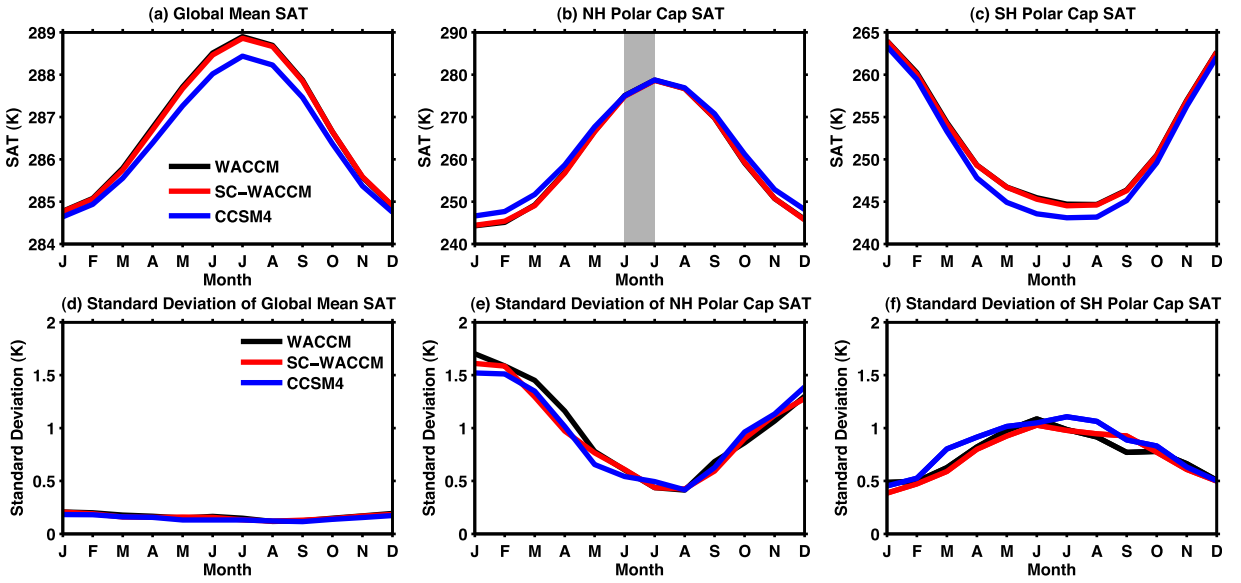

Figure 12. Surface air temperature (SAT) in WACCM (black), SC-WACCM (red), and CCSM4 (blue) as a function of month. (a) Global mean, (b) Northern Hemisphere (NH) polar cap average, and (c) Southern Hemisphere polar cap average (SH). Months when CCSM4 is not significantly different from WACCM at the 95% level are highlighted with gray shading. (d, e, and f) as Figures 12a, 12b, and 12c but for the standard deviation of SAT.

WACCM over the Northern Hemisphere polar cap in winter also reflect the differences in sea ice, with CCSM4 having less extensive Arctic sea ice than WACCM.

Figures 12d–12f show the standard deviations for each latitude band and each model. The standard deviation is reasonably similar across all three models but is much larger at the poles than in the global mean.

We also show the zonal mean *SAT*, *SLP* and precipitation for DJF and JJA as a function of latitude in Figure 13. WACCM and SC-WACCM, again, show little difference for all fields in both seasons. The main differences between WACCM/SC-WACCM and CCSM4, particularly the differences in extratropical *SLP*, likely reflect the differences in horizontal resolution and the TMS parameterization, as discussed above.

Despite the very different treatment of chemical processes in WACCM and SC-WACCM, we find no significant difference in the simulation of the surface climate in the two integrations under preindustrial conditions. The surface climate of WACCM/SC-WACCM differs significantly from CCSM4 but is qualitatively similar except in sea ice extent and extratropical SLP.

Table 2. Stratospheric Sudden Warming (SSW) Benchmarks Following *Charlton and Polvani* [2007] for WACCM, SC-WACCM, and CCSM4[a]

SSW Benchmarks	WACCM (N = 97)	SC-WACCM (N = 83)	CCSM4 (N = 4)
Frequency (SSWs year^{-1})	0.5 (0.04)	0.4 (0.04)	0.08 (0.1)
ΔT_{10} (K)	9.1 (0.4)	9.1 (0.4)	6.5 (0.5)
ΔT_{100} (K)	2.6 (0.1)	2.6 (0.1)	2.8 (0.7)
ΔU_{10} (m s^{-1})	22.7 (0.9)	23.5 (1.1)	36.7 (8.6)
$\Delta v^* T^*_{100}$ (m K s^{-1})	10.2 (0.6)	9.7 (0.6)	8.4 (2.1)
$\Delta NAMI_{1000}$	−0.2 (0.06)	−0.2 (0.08)	−0.2 (0.4)

[a]Standard errors are listed in parentheses. Note: the central date of a SSW is defined as the first day when the zonal mean stratospheric westerlies become easterly at 60°N and 10hPa. ΔT_{10}: The area-weighted mean 10 hPa polar cap temperature anomaly, 90°–50°N, ±5 days from the central date; ΔT_{100}: The area-weighted mean 100 hPa polar cap temperature anomaly, ±5 days from the central date; ΔU_{10}: The difference in zonal mean zonal wind, at 60°N and 10 hPa, 15–5 days prior to the central date minus 0–5 days after the central date; $\Delta v^* T^*_{100}$: The area-weighted, mean, 100 hPa $v^* T^*$ anomaly, 45°–75°N 20–0 days before the central date; and $\Delta NAMI_{1000}$: The mean, 1000 hPa NAM index, 10–60 days after the central date.

4.4. Climate Variability

Beyond comparing the mean climate of the WACCM and SC-WACCM integrations, we are also interested in how well SC-WACCM simulates atmospheric variability relative to WACCM. Here we focus on only a few metrics that characterize the important features of the variability in these integrations, with emphasis on the dynamical coupling between the stratosphere and troposphere.

Figures 14a and 14b show the probability density distributions for zonal mean (a) meridional

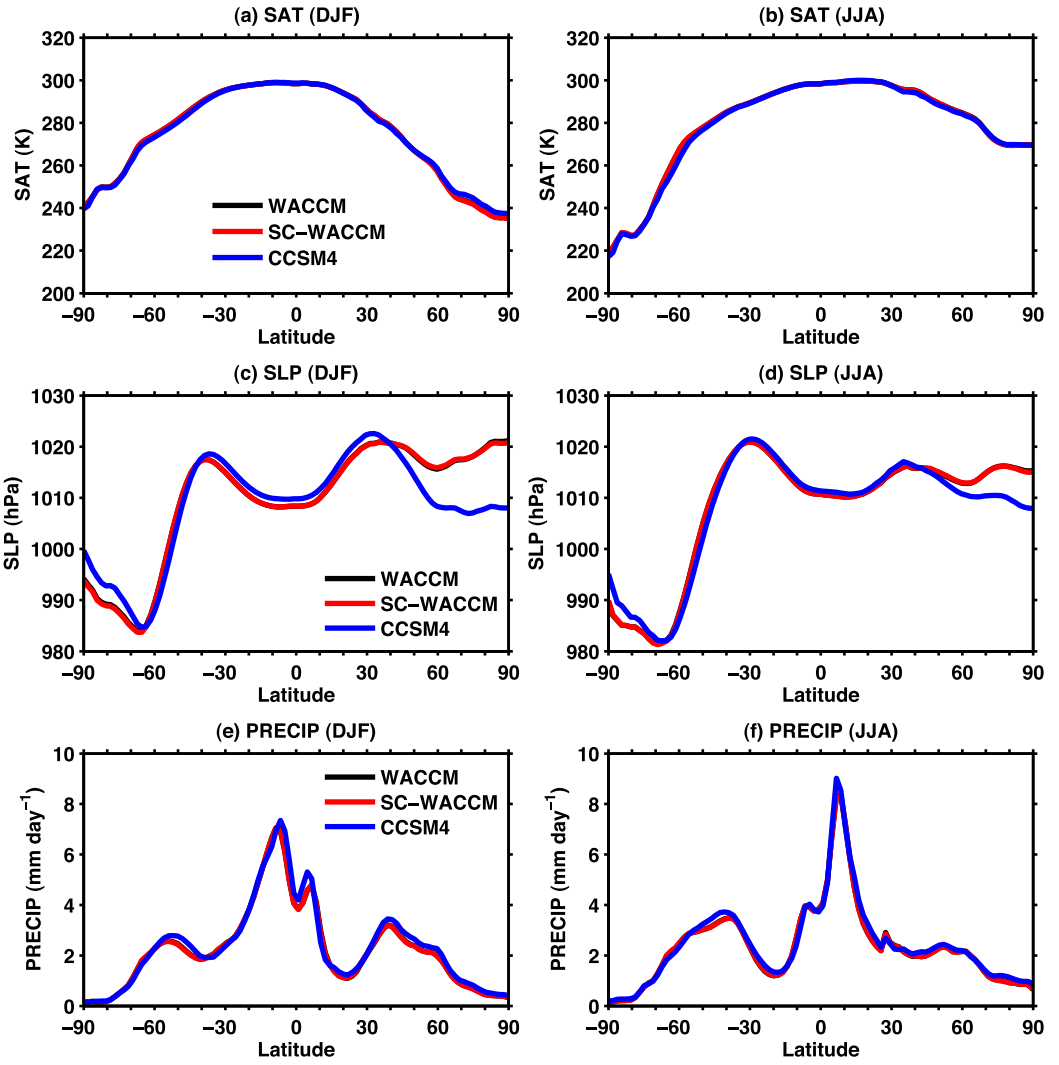

Figure 13. Zonal mean (a, b) surface air temperature (SAT), (c, d) sea-level pressure (SLP), and (e, f) precipitation (PRECIP) for December-January-February (DJF) (Figures 13a, 13c, and 13e) and June-July-August (JJA) (Figures 13b, 13d, and 13f). Black, red, and blue curves are WACCM, SC-WACCM, and CCSM4.

eddy heat flux at 10 hPa averaged from 45°N to 75°N and (b) polar cap averaged temperature at 10 hPa for WACCM, SC-WACCM and CCSM4, for the winter season, DJFM. We use the meridional eddy heat flux as a proxy for the vertical component of the wave activity flux. The heat flux and temperature distributions look very similar in WACCM and SC-WACCM. The CCSM4 distribution for heat flux is significantly narrower (by a K-S test), showing a much weaker tail of high positive values while the temperature distribution illustrates the cold polar cap stratospheric temperature bias in CCSM4 relative to WACCM that accompanies the strong zonal mean zonal winds (Figure 9a).

Figures 14c and 14d are identical to Figures 14a and 14b except that they show the heat flux and temperature anomalies, i.e., the deviations from the climatological means. Again, the heat flux and temperature anomaly distributions for WACCM and SC-WACCM are qualitatively similar. Note how the CCSM4 distribution for heat flux anomalies is narrower than the WACCM/SC-WACCM distributions. After removing the bias in CCSM4 temperature, we see a clear lack of skewness in the CCSM4 temperatures relative to WACCM and SC-WACCM. This lack of large positive temperature anomalies in CCSM4 reflects weaker heat fluxes and the consequent absence of extreme coupling events, such as SSWs, which we discuss next.

Table 2 lists a series of composite mean benchmarks for SSWs for WACCM, SC-WACCM and CCSM4 (± the standard error) following the definitions in *Charlton and Polvani* [2007] (see Table 2 caption for benchmark descriptions). The frequency of SSWs is slightly greater in WACCM compared to SC-WACCM, 0.5 per year

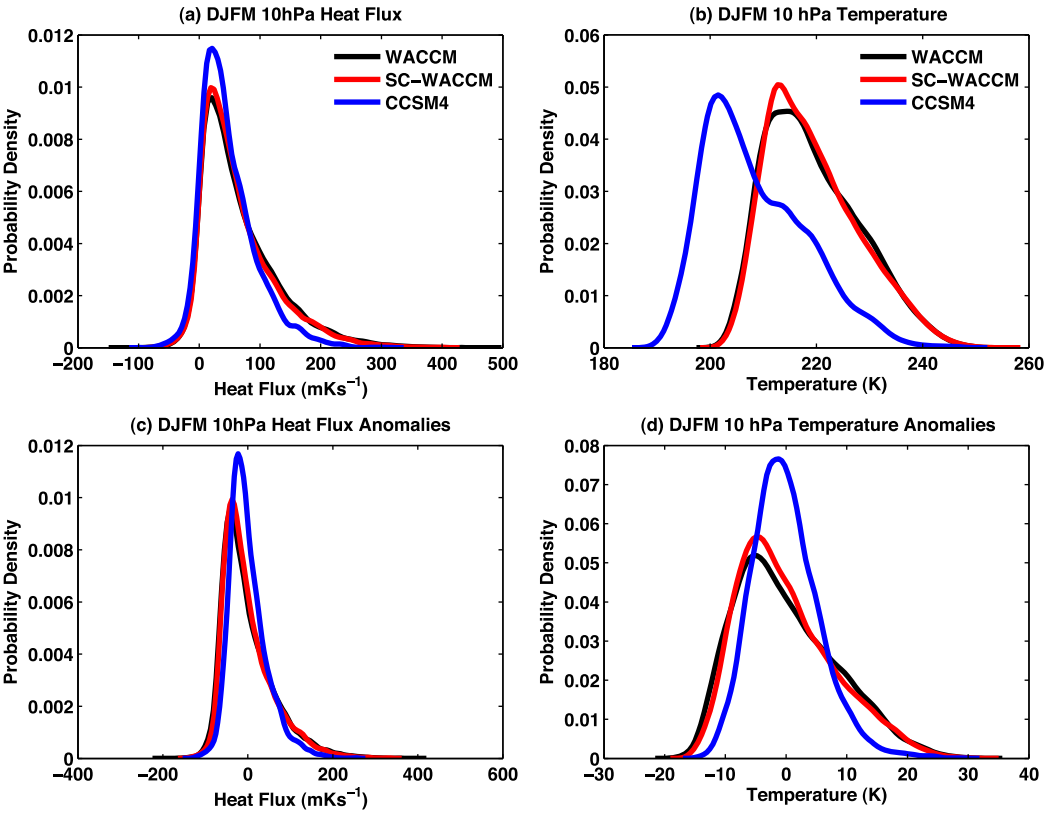

Figure 14. Probability density distributions of 10 hPa December-January-Febraury-March (DJFM) (a) total and (c) anomalous zonal mean meridional eddy heat flux averaged from 45° to 75°N, (b) total and (d) anomalous polar cap averaged temperature. Black, red and blue curves are WACCM, SC-WACCM and CCSM4. Probability density distributions are computed using a kernel density estimator, which performs a nonparametric, smoothed fit to the data.

versus 0.4 per year, yet the characteristics of the warmings, described by the other benchmarks, are very similar. The WACCM and SC-WACCM benchmark values also compare reasonably well with observations with the exception of the benchmark which characterizes the surface Northern Annular Mode (NAM) signal following SSWs, $\Delta NAMI_{1000}$. The NAM is the leading mode of Northern Hemisphere extratropical atmospheric variability and many studies have shown that the zonal mean tropospheric signature following extreme stratospheric events projects onto the NAM [*Baldwin and Dunkerton*, 2001]. Assuming climate change since 1850 has not changed model variability, the $\Delta NAMI_{1000}$ benchmark appears weaker in the models, suggesting weaker stratosphere-troposphere coupling. The frequency of SSWs in CCSM4 is much lower than WACCM and SC-WACCM, and the other benchmarks show some inconsistencies with the other two models. Because there are so few SSWs in CCSM4, the composite mean benchmarks are dominated by a single very large warming and should not be overinterpreted.

Another important feature of SSW climatology is the seasonal distribution of SSWs. Figure 15 shows the frequency of SSWs as a function of month for WACCM, SC-WACCM and CCSM4. The seasonal cycle of SSWs is not significantly different between WACCM and SC-WACCM while CCSM4 SSWs are confined to the late winter. The observed seasonal distribution of SSWs shows the highest frequency in January and February (approximately 0.2 SSWs per year), which agrees well with the WACCM and SC-WACCM distributions shown here for preindustrial conditions. See *Marsh et al.* [2013] and *de la Torre*

Table 3. Timing and Performance of Preindustrial Control Simulations on the Yellowstone Supercomputer[a]

Model	Cores	Simulated Years/Day	Core Hours/ Simulated Year
WACCM	352	7.5	1130
SC-WACCM	352	14.8	573
CCSM4 1°	352	19.6	432
CCSM4 2°	416	42.0	237

[a]Yellowstone computation nodes use the Intel Xeon E5–2670 (Sandy Bridge) 2.6 GHz processor, each containing 8 cores.

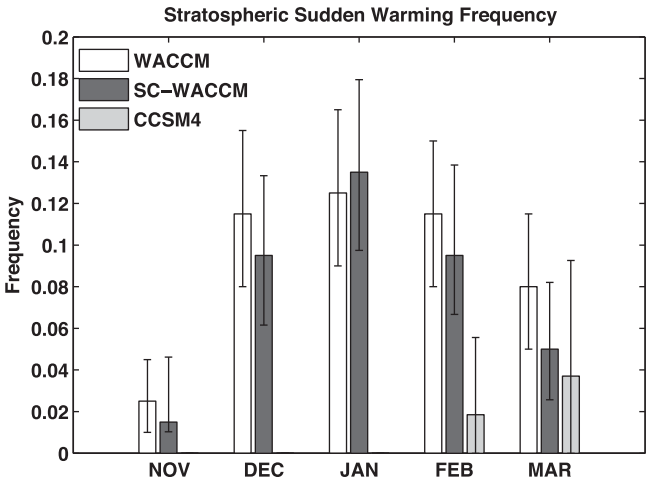

Figure 15. Stratospheric sudden warming (SSW) frequency in SSW per year as a function of month for WACCM, SC-WACCM and CCSM4. 95% confidence intervals are calculated using bootstrapping.

et al. [2012] for a detailed comparison of WACCM and CCSM4 SSWs with reanalysis data for integrations over the historical period.

Given that there appears to be a small reduction in variability in the stratosphere when ozone is prescribed versus computed interactively, we now examine whether there are any differences in tropospheric variability that may result from or contribute to the differences in stratospheric variability. Just as stratospheric variability has been frequently linked to zonal mean tropospheric variability, i.e., the NAM, it is linked to zonally *asymmetric* tropospheric variability in the North Atlantic region. Specifically, downward migrating stratospheric anomalies tend to project onto the large-scale mode of tropospheric variability known as the North Atlantic Oscillation (NAO) [*Scaife*, 2005; *Shaw and Perlwitz*, 2013; *Smith and Polvani*, 2014]. Figure 16 shows the probability density distribution of the normalized NAO index for the three models. There are no significant differences between the distributions (there are also no significant differences for the nonnormalized NAO indices, not shown). Thus, prescribed chemistry does not seem to have a significant impact on the variability of the North Atlantic region and, while, stratosphere-troposphere coupling projects onto the NAO, the more realistic representation of this process in the stratosphere-resolving models, WACCM and SC-WACCM, does not appear to significantly alter their NAO distributions relative to CCSM4.

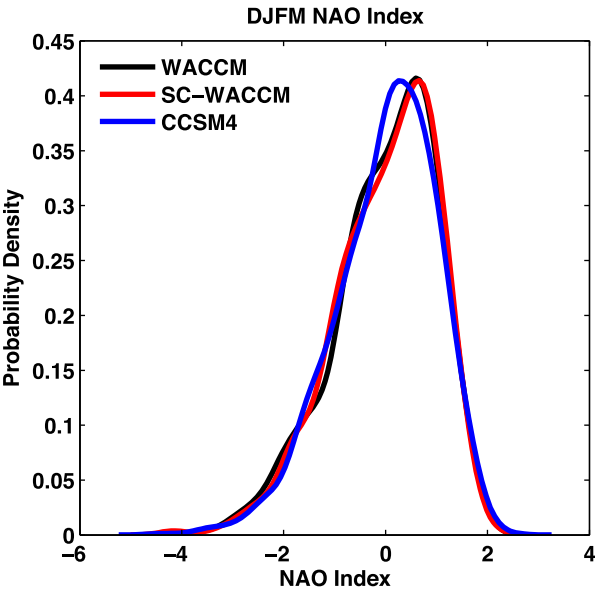

Figure 16. Probability density distributions of the North Atlantic Oscillation (NAO) index. Black, red and blue curves are WACCM, SC-WACCM and CCSM4. The NAO index is the time series of the leading EOF of monthly sea-level pressure anomalies for the North Atlantic region, 20°–90°N and 90°W–30°E. Probability density distributions are computed using a kernel density estimator, which performs a nonparametric, smoothed fit to the data.

Finally, we compare metrics of El Niño-Southern Oscillation (ENSO) variability across the three models. Figure 17a shows the mean power spectral density of the monthly Niño 3.4 Index for 50 year segments of the time series (thick lines); the individual spectra for each 50 year segment are shown in the thin lines. As expected, the peak power spectral density lies within the 3–5 year range for each model. The spread of the thin lines illustrates that although there are differences in the mean power spectra across the models, there is quite a bit of variability within each model. However, the probability density distributions in Figure 17b show that the distribution of the Niño 3.4 Index in DJF is significantly narrower in CCSM4 than in WACCM and SC-WACCM which is consistent with the weaker peak in power spectral density in CCSM4 in Figure 17a. Horizontal resolution may have an influence on ENSO variability.

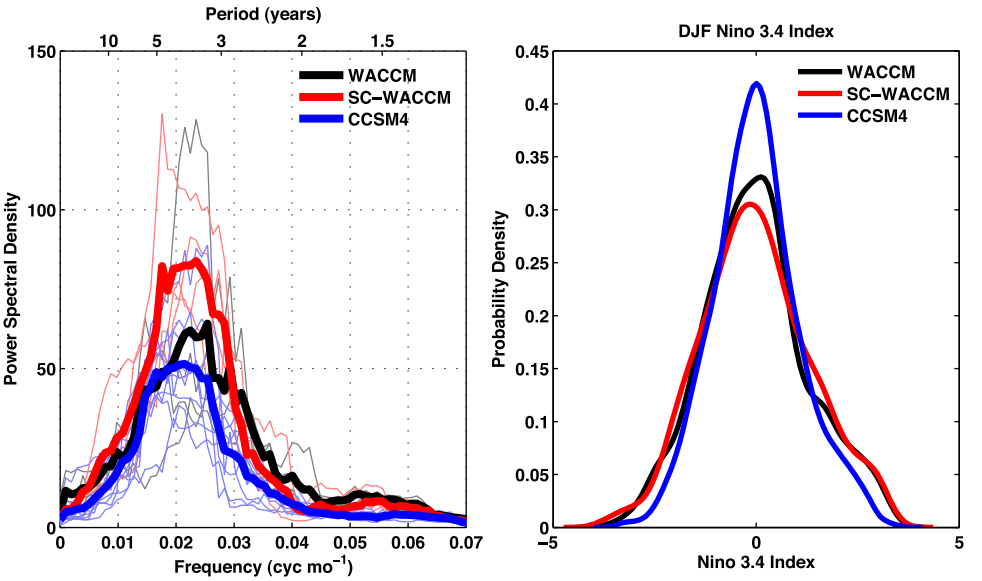

Figure 17. (a) Mean power spectrum and (b) probability density distributions of the NINO 3.4 index for WACCM (black), SC-WACCM (red) and CCSM4 (blue). Thin gray, pink and blue lines in Figure 17a show individual 50 year spectra for WACCM, SC-WACCM, and CCSM4, respectively. The NINO 3.4 index is the time series of sea surface temperature anomaly averaged over the tropical Pacific region, 5°S–5°N and 170°W–120°W.

5. Computational Costs

We have now shown that SC-WACCM simulates a climate that is almost indistinguishable from WACCM. By specifying the chemistry in SC-WACCM, we have maintained a good representation of the climate, while eliminating the computational cost required to calculate middle atmosphere chemistry interactively.

The computational cost and typical simulated years per day of SC-WACCM, relative to WACCM and CCSM4, are presented in Table 3. SC-WACCM is approximately half the cost and can achieve twice the throughput of WACCM on the NCAR Yellowstone supercomputer using 352 processor cores. Relative to CCSM4, it is 1.3 times more expensive than the 1° version, and 2.4 times more expensive than the 2° version. The latter ratio mostly roughly reflects the additional number of levels in SC-WACCM, i.e., 66 versus 26.

Thus, SC-WACCM provides users of the CESM1 community models with a stratosphere-resolving global climate model, well suited for studies of stratospheric dynamics and stratosphere-troposphere interactions, at half the computational cost of WACCM and with superior stratospheric circulation and variability to CCSM4.

6. Discussion and Conclusions

In this study, we have compared the mean climate and variability of two preindustrial integrations: the first using the standard WACCM with interactive middle atmosphere chemistry and the second with SC-WACCM, the new configuration of WACCM with specified chemistry.

The largest differences between WACCM and SC-WACCM occur as a result of prescribing monthly mean (i.e., temporally smoothed) ozone and chemical and shortwave heating rates in SC-WACCM. Note that we are not doing anything unusual here; prescribing monthly mean, zonal mean ozone is standard practice for all of the CMIP5-class GCMs without interactive chemistry. Using monthly averages leads to two issues: (1) the absence of a diurnal cycle in ozone and (2) a weakening of the seasonal cycle of chemical and shortwave heating rates due to linear interpolation from monthly to daily mean fields. The first issue causes SC-WACCM to have warmer temperatures in the lower mesosphere compared to WACCM because ozone concentrations in WACCM are lowest during daylight hours and thus, WACCM absorbs less shortwave radiation than SC-WACCM. The second issue causes large differences in chemical and shortwave heating rates in the thermosphere. Although these differences in heating rates are large, the percentage differences are less than ±5% due to large climatological heating rates in the thermosphere.

In spite of these differences, in the lower stratosphere and troposphere, WACCM and SC-WACCM have almost identical climatologies. We examined the zonal mean temperatures and winds, the seasonal evolution of the polar vortices, the Brewer-Dobson circulation and the tropical water vapor tape recorder, all of which show remarkable similarities between the two models. At the surface, the mean climate of WACCM and SC-WACCM, diagnosed using surface air temperature, sea-level pressure, precipitation and sea ice extent, are also indistinguishable. Thus, prescribing middle atmosphere chemistry in SC-WACCM does not appear to degrade the simulation of the mean climate of the lower stratosphere, troposphere and surface relative to WACCM.

Perhaps more surprisingly, we found that the stratospheric variability in both WACCM and SC-WACCM is also comparable. We examined the probability density distributions of stratospheric meridional eddy heat fluxes and temperatures and found only small differences. Consequently, the frequency, seasonal distribution and composite characteristics of stratospheric sudden warmings are also similar across the two models. In the troposphere, we limited our analysis to the NAO and ENSO and again found no significant difference between WACCM and SC-WACCM.

Throughout the paper, we also presented CCSM4 diagnostics along with the WACCM and SC-WACCM diagnostics as a means of comparing stratosphere-resolving ("high-top") and non-stratosphere-resolving ("low-top") models. Although it is not a clean "high-top"-"low-top" comparison, since CCSM4 has other configurational differences, such as a finer horizontal resolution and differences in physical parameterizations such as turbulent mountain stress (TMS) and gravity waves, we included these diagnostics because CCSM4 is the main scientifically validated configuration of CESM1 for CMIP5. There are clear differences between the "high-top" models, WACCM and SC-WACCM, and CCSM4, notably the lack of stratospheric variability in CCSM4 in the Northern Hemisphere. At the surface, the lack of TMS in CCSM4 results in weaker (stronger) sea-level pressures in the Northern (Southern) Hemisphere extratropics and less (more) extensive Arctic (Antarctic) sea ice.

The aim of this paper was to describe SC-WACCM and contrast its simulated climate and variability with WACCM. Beyond issues associated with temporal smoothing of the prescribed ozone and chemical and shortwave heating fields, we find that interactive stratospheric chemistry appears to have little influence on the simulated mean climate and variability in WACCM under preindustrial conditions. This is true even in the lower and middle stratosphere, where ozone chemistry is most active. Given that the radiative timescales associated with ozone are longer than the dynamical timescales in the lower/middle stratosphere, the agreement between WACCM and SC-WACCM is not entirely surprising.

We emphasize here that SC-WACCM is not intended for studying the dynamics of the upper atmosphere (above the radiative transfer overlap region near 65 km) as the physics and chemistry in that region are simplified in this model. However, our analysis shows that SC-WACCM is suitable for studies of stratospheric dynamics and stratosphere-troposphere coupling, the important advantage being that SC-WACCM runs approximately twice as fast and at half the computational cost of WACCM (Table 3).

Acknowledgments

KLS is funded by a Natural Sciences and Engineering Research Council of Canada (NSERC) Postdoctoral Fellowship. LMP is supported in part by a grant from the U.S. National Science Foundation (NSF) to Columbia University. RRN is funded by the Advanced Study Program at NCAR. The CESM project is supported by the NSF and the Office of Science (BER) of the U.S. Department of Energy (DOE). The authors acknowledge the Climate Simulation Laboratory at NCAR's Computational and Information Systems Laboratory (CISL; sponsored by NSF and other agencies) and the NOAA Research and Development High Performance Computing Program for providing computing and storage resources that have contributed to the research results reported within this paper. The CMIP5 WACCM preindustrial integrations are publicly available on the DOE Program for Climate Model Diagnosis and Intercomparison (PCMDI) Earth System Grid Federation (ESGF) website and the SC-WACCM preindustrial integrations are available upon request.

References

Albers, J. R., and T. R. Nathan (2012), Pathways for communicating the effects of stratospheric ozone to the polar vortex: Role of zonally asymmetric ozone, *J. Atmos. Sci.*, *69*(3), 785–801, doi:10.1175/JAS-D-11-0126.1.

Albers, J. R., J. P. McCormack, and T. R. Nathan (2013), Stratospheric ozone and the morphology of the northern hemisphere planetary waveguide, *J. Geophys. Res. Atmos.*, *118*, 563–576, doi:10.1029/2012JD017937.

Baldwin, M. P., and T. J. Dunkerton (2001), Stratospheric harbingers of anomalous weather regimes, *Science*, *294*, 581–584.

Brasseur, G. P., and S. Solomon (2005), *Aeronomy of the Middle Atmosphere*, 3rd ed., 646 pp., Springer, Dordrecht, Netherlands.

Butchart, N., et al. (2010), Chemistry-climate model simulations of twenty-first century stratospheric climate and circulation changes. *J. Clim.*, *23*, 5349–5374.

Charlton, A. J., and L. M. Polvani (2007), A new look at stratospheric sudden warmings. Part I: Climatology and modeling benchmarks, *J. Clim.*, *20*, 449–469.

Charlton-Perez, A. J., et al. (2013), On the lack of stratospheric dynamical variability in low-top version of the CMIP5 models, *J. Geophys. Res. Atmos.*, *118*, 2494–2505, doi:10.1002/jgrd.50125.

Collins, W. D., et al. (2004), *Description of the NCAR Community Atmosphere Model (CAM3)*, Natl. Cent. for Atmos. Res., Boulder, Colo.

Crook, J. A., N. P. Gillett, and S. P. E. Keeley (2008), Sensitivity of Southern Hemisphere climate to zonal asymmetry in ozone, *Geophys. Res. Lett.*, *35*, L07806, doi:10.1029/2007GL032698.

de la Torre, L., R. R. Garcia, D. Barriopedro, and A. Chandran (2012), Climatology and characteristics of stratospheric sudden warmings in the Whole Atmosphere Community Climate Model, *J. Geophys. Res.*, *117*, D04110, doi:10.1029/2011JD016840.

Fomichev, V. I., J. P. Blanchet, and D. S. Turner (1998), Matrix parameterization of the 15 μm co_2 band cooling in the middle and upper atmosphere for variable co_2 concentration, *J. Geophys. Res.*, *103*, 11,505–11,528.

Gabriel, A., D. Peters, I. Kirchner, and H.-F. Graf (2007), Effect of zonally asymmetric ozone on stratospheric temperature and planetary wave propagation, *Geophys. Res. Lett.*, *34*, L06807, doi:10.1029/2006GL028998.

Garcia, R. R., and W. J. Randel (2008), Acceleration of the Brewer-Dobson circulation due to increases in greenhouse gases, *J. Atmos. Sci.*, *65*, 2731–2739, doi:10.1175/2008JAS2712.1.

Garcia, R. R., and S. Solomon (1994), A new numerical model of the middle atmosphere: 2. Ozone and related species. *J. Geophys. Res.*, *99*, 12,937–12,951, doi:10.1029/94JD00725.

Gent, P. R., et al. (2011), The Community Climate System Model Version 4, *J. Clim.*, *24*(19), 4973–4991, doi:10.1175/2011JCLI4083.1.

Gillett, N. P., J. F. Scinocca, D. A. Plummer, and M. C. Reader (2009), Sensitivity of climate to dynamically-consistent zonal asymmetries in ozone, *Geophys. Res. Lett.*, *36*, L10809, doi:10.1029/2009GL037246.

Hardiman, S. C., N. Butchart, and N. Calvo (2013), The morphology of the BrewerDobson circulation and its response to climate change in CMIP5 simulations. *Q. J. R. Meteorol. Soc.*, doi:10.1002/qj.2258.

Haynes, P. H., C. J. Marks, M. E. McIntyre, T. G. Shepherd, and K. P. Shine (1991), On the "Downward Control" of extratropical diabatic circulations by eddy-induced mean zonal forces, *J. Atmos. Sci.*, *48*(4), 651–678.

Hurrell, J. W., et al. (2013), The Community Earth System Model: A framework for collaborative research, *Bull. Am. Meteorol. Soc.*, *94*, 1339–1360, doi:10.1175/BAMS-D-12-00121.1.

Kockarts, G. (1980), Nitric oxide cooling in the terrestrial thermosphere, *Geophys. Res. Lett.*, *7*, 137–140.

Lamarque, J.-F., G. P. Kyle, M. Meinshausen. K. Riahi, S. J. Smith, D. P. van Vuuren, A. Conley, F. Vitt (2011), Global and regional evolution of short-lived radiatively-active gases and aerosols in the representative concentration pathways, *Clim. Change*, *109*, 191–212, doi:10.1007/s10584-011-0155-0.

Lamarque, J.-F., et al. (2012), CAM-chem: Description and evaluation of interactive atmospheric chemistry in the Community Earth System Model, *Geosci. Model Dev.*, *5*, 369–411, doi:10.5194/gmd-5–369-2012.

Marsh, D. R., R. R. Garcia, D. E. Kinnison, B. A. Bouville, F. Sassi, S. C. Solomon, and K. Matthes (2007), Modeling the whole atmosphere response to solar cycle changes in radiative and geomagnetic forcing, *J. Geophys. Res.*, *112*, D23306, doi:10.1029/2006JD008306.

Marsh, D. R., M. J. Mills, D. E. Kinnison, J.-F. Lamarque, N. Calvo, and L. M. Polvani (2013), Climate Change from 1850 to 2005 Simulated in CESM1(WACCM), *J. Clim.*, *26*(19), 7372–7391, doi:10.1175/JCLI-D-12-00558.1.

Meinshausen, M., et al. (2011), The RCP greenhouse gas concentrations and their extensions from 1765 to 2300, *Clim. Change*, *109*, 213–241, doi:10.1007/s10584-011-0156-z.

McCormack, J. P., T. R. Nathan, and E. C. Cordero (2011), The effect of zonally asymmetric ozone heating on the Northern Hemisphere winter polar stratosphere, *Geophys. Res. Lett.*, *38*, L03802, doi:10.1029/2010GL045937.

Mlynczak, M. G., and S. Solomon (1993), A detailed evaluation of the heating efficiency in the middle atmosphere, *J. Geophys. Res.*, *98*, 10,517–10,541, doi:10.1029/93JD00315.

Neale, R. B., et al. (2012), Description of the NCAR Community Atmosphere Model (CAM 5.0), *NCAR Tech. Note NCAR/TN-486+STR*, Natl. Cent. for Atmos. Res., Boulder, Colo.

Previdi, M., and L. M. Polvani (2014), Climate system response to stratospheric ozone depletion and recovery, *Q. J. R. Meteorol. Soc.*, doi:10.1002/qj.2330.

Richter, J. H., F. Sassi, and R. R. Garcia (2010), Toward a physically based gravity wave source parameterization in a general circulation model, *J. Atmos. Sci.*, *67*(1), 136–156, doi:10.1175/2009JAS3112.1.

Sassi, F. (2005), The effects of interactive ozone chemistry on simulations of the middle atmosphere, *Geophys. Res. Lett.*, *32*, L07811, doi:10.1029/2004GL022131.

Scaife, A. A. (2005), A stratospheric influence on the winter NAO and North Atlantic surface climate, *Geophys. Res. Lett.*, *32*, L18715, doi:10.1029/2005GL023226.

Shaw, T. A., and J. Perlwitz (2013), The life cycle of Northern Hemisphere downward wave coupling between the stratosphere and troposphere, *J. Clim.*, *26*(5), 1745–1763, doi:10.1175/JCLI-D-12-00251.1.

Smith, K. L., and L. M. Polvani (2014), The impacts of Arctic stratospheric ozone anomalies, *Environ. Res. Lett.*, *9*, 074015, doi:10.1088/1748–9326/9/7/074015.

SPARC CCMVal (2010), V. Eyring, T. G. Shepherd, D. W. Waugh (Eds.), SPARC report on the evaluation of chemistry-climate models, *SPARC Rep. 5, WCRP-132, WMO/TD 1526*.

Tegtmeier, S., M. Rex, I. Wohltmann, and K. Krüger (2008), Relative importance of dynamical and chemical contributions to Arctic wintertime ozone, *Geophys. Res. Lett.*, *35*, L17801, doi:10.1029/2008GL034250.

Thompson, D. W. J., S. Solomon, P. J. Kushner, M. H. England, K. M. Grise, and D. J. Karoly (2011), Signatures of the Antarctic ozone hole in Southern Hemisphere surface climate change, *Nat. Geosci.*, *4*(11), 741–749, doi:10.1038/ngeo1296.

Waugh, D. W., L. Oman, P. a. Newman, R. S. Stolarski, S. Pawson, J. E. Nielsen, and J. Perlwitz (2009), Effect of zonal asymmetries in stratospheric ozone on simulated Southern Hemisphere climate trends, *Geophys. Res. Lett.*, *36*, L18701, doi:10.1029/2009GL040419.

Young, P. J., et al. (2013), Pre-industrial to end 21st century projections of tropospheric ozone from the Atmospheric Chemistry and Climate Model Intercomparison Project (ACCMIP), *Atmos. Chem. Phys.*, *13*, 2063–2090, doi:10.5194/acp-13-2063-2013.